Learning Contrastive Embedding in Low-Dimensional Space

Shuo Chen[†], Chen Gong[§], Jun Li[§], Jian Yang[§], Gang Niu[†], Masashi Sugiyama[‡]

Abstract

Contrastive learning (CL) pretrains feature embeddings to *scatter* instances in the feature space so that the training data can be well discriminated. Most existing CL techniques usually encourage learning such feature embeddings in the *high-dimensional space* to maximize the instance discrimination. However, this practice may lead to undesired results where the scattering instances are *sparsely distributed* in the high-dimensional feature space, making it difficult to capture the underlying similarity between pairwise instances. To this end, we propose a novel framework called *contrastive learning with low-dimensional reconstruction* (CLLR), which adopts a regularized projection layer to *reduce* the dimensionality of the feature embedding. In CLLR, we build the *sparse/low-rank* regularizer to adaptively reconstruct a low-dimensional projection space while preserving the basic objective for instance discrimination, and thus successfully learning contrastive embeddings that alleviate the above issue. Theoretically, we prove a tighter error bound for CLLR; empirically, the superiority of CLLR is demonstrated across multiple domains. Both theoretical and experimental results emphasize the significance of learning low-dimensional contrastive embeddings.

1 Introduction

Recently, unsupervised learning approaches have been greatly promoted by the *contrastive learning* (CL), which shows encouraging performance compared to fully supervised approaches [8, 21]. CL pretrains deep neural networks with unlabeled instances, and the learned feature embeddings can be directly used to extract features from the raw data [35]. Thereby, CL has been successfully applied in many downstream recognition tasks such as classification [42], retrieval [41], and clustering [3].

As an unsupervised learning problem setting where the human annotation is not available, CL approaches usually consider building the *pseudo supervision* in their learning objectives [36, 19], and thus CL is also regarded as a *self-supervised learning* approach. Originally, the pseudo supervision of CL is to push away each pair of instances to scatter data points in the feature space, by which all instances in the training data can be well discriminated (*i.e.*, the *instance discrimination*) [14, 40]. This original design has been empirically validated to be particularly effective in the representation learning [28, 6], and has also been theoretically proved to approximate an *unbiased* supervised learning objective [32, 11]. Many recent efforts have increasingly focused on two different directions to further improve the performance of CL. The first one is to introduce plentiful data-augmentation

---

[†]S. Chen and G. Niu are with RIKEN Center for Advanced Intelligence Project (AIP), Japan (E-mail: {shuo.chen.ya@riken.jp, gang.niu.ml@gmail.com}).

[§]C. Gong, J. Li, and J. Yang are with the PCA Lab, Key Lab of Intelligent Perception and Systems for High-Dimensional Information of Ministry of Education, and Jiangsu Key Lab of Image and Video Understanding for Social Security, School of Computer Science and Engineering, Nanjing University of Science and Technology, China (E-mail: {junli, chen.gong, csjyang}@njust.edu.cn).

[‡]M. Sugiyama is with RIKEN Center for Advanced Intelligence Project (AIP), Japan; and also with the Graduate School of Frontier Sciences, The University of Tokyo, Japan (E-mail: sugi@k.u-tokyo.ac.jp).

to generate the *positive pair* which consists of each instance and its perturbation [35, 28]. Then, any two instances in the training data are regarded as the *negative pair*, and the objective of *metric learning* [33, 43] can be used to learn feature embeddings that distinguish positive pairs and negative pairs. Nevertheless, the negative pairs built in CL are inherently noisy because they contain false negatives consisted of semantically similar instances [30]. Therefore, the second way to improve the performance of CL is to reduce the impact of false negative pairs. To this end, some recent works convert it to *positive-unlabeled learning* [11, 27] and clustering problems [3, 46] to reweight the importance of negative pairs, and thus constraining the undesired repelling of negative pairs [3, 46].

Although the existing methods have achieved promising results to some extent, their reliabilities highly depend on the effectiveness of instance discrimination [20, 32]. However, recent works usually encourage learning contrastive embedding in *high-dimensional space* to maximally discriminate instances, so that the dimensionality of self-supervised contrastive embedding [7, 9] is set to be much larger than the dimensionality of traditional fully supervised embedding [10, 44]. This practice makes data points *sparsely distribute* in the feature space (which is similar to the *curse of dimensionality* [18]), and thereby the corresponding CL methods may fail to capture the intrinsic similarity between pairwise instances. Such a problem can hardly be solved by simply setting a low dimensionality for the output layer, as it will cause the *dimensional collapse* with insufficient instance discrimination [20]. Some popular compression approaches such as distillation techniques [5, 47] enable us to train small networks under the supervision of original contrastive embeddings, yet the improper similarity predictions can still be inherited from the original networks. Therefore, a new CL method is desired to effectively learn the low-dimensional feature embedding.

In this paper, we propose a novel framework dubbed *contrastive learning with low-dimensional reconstruction* (CLLR) to explicitly address the above issue caused by the high dimensionality in CL. Specifically, we introduce a new sparse projection layer to reconstruct the features of instances in low-dimensional space and meanwhile scatter all instances in the original high-dimensional space (see Fig. 1). Then, we obtain the low-dimensional contrastive embedding which can also effectively distinguish instances in the training data. Theoretically, we prove a lower bound for the min-max distance ratio of the learned contrastive embedding, which ensures that CLLR can better capture the instance similarity than the existing CL models.

Figure 1: Conceptual illustration of our proposed CLLR. In our method, we discriminate all instances in high-dimensional space and introduce a sparse projection layer (the red part) to reconstruct the features of instances in the low-dimensional latent space.

Experimentally, our approach consistently improves the state-of-the-art methods on vision, language, and reinforcement learning benchmarks. To the best of our knowledge, we are the first to propose learning the original contrastive embedding in low-dimensional space. The proposed method is very generic, so it can be applied in many existing CL models. Our main contributions are summarized as: **I).** we propose a novel framework to enhance the generalization ability of contrastive learning via introducing a sparse / low-rank regularized projection layer to adaptively reduce the high dimensionality of contrastive embedding; **II).** we establish complete theoretical guarantees for our method by analyzing the error bound of distance predictions and the convergence of the learning algorithm, respectively; **III).** we conduct extensive experiments on real-world datasets to validate the superiority of our method over the state-of-the-art CL approaches, and the results consistently emphasize the necessity / significance of learning low-dimensional contrastive embeddings.

Notations. We write matrices and vectors as bold uppercase characters and bold lowercase characters, respectively. We denote the training dataset $\mathcal{X} = \{\boldsymbol{x}_i \in \mathbb{R}^m | i = 1, 2, \ldots, N\}$ where m is the data dimensionality and N is the sample size. Operators $\|\cdot\|_2$, $\|\cdot\|_{2,1}$, and $\|\cdot\|_*$ denote the vector/matrix ℓ_2-norm, $\ell_{2,1}$-norm (*i.e.*, the sum of ℓ_2-norm for columns), and nuclear-norm, respectively.

1.1 Background & Related Work

In this subsection, we briefly review the background of contrastive learning and the related work.
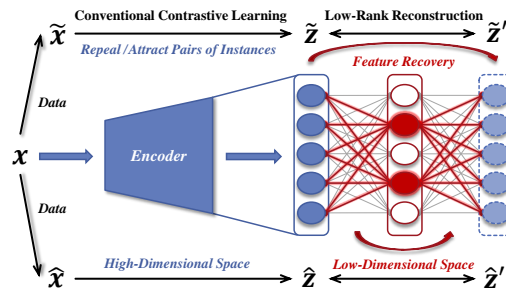
Instance Discrimination & Contrastive Learning. As a popular unsupervised / self-supervised learning approach, the basic goal of contrastive learning (CL) algorithm is to learn a generic feature embedding $\boldsymbol{\Phi}\colon \mathbb{R}^m \mapsto \mathbb{R}^H$, which transforms the data point from m-dimensional sample space to H-dimensional embedding space. The primitive CL method called instance discrimination learns such an embedding by directly enlarging the following distance between each pair of two instances $\boldsymbol{x}_i$ and $\boldsymbol{x}_j$ in the training data [14, 40]

$$\mathcal{D}_{\boldsymbol{\Phi}}(\boldsymbol{x}_i, \boldsymbol{x}_j) = \|\boldsymbol{\Phi}(\boldsymbol{x}_i) - \boldsymbol{\Phi}(\boldsymbol{x}_j)\|_2 / H, \tag{1}$$

where H is the dimensionality of the learned feature embedding. The design philosophy for instance discrimination is that when we scatter all instances in the feature space, the characteristic of each instance are captured and thus the training data can be well memorized by the neural network [20]. When we further generate the positive pairs $(\boldsymbol{x}, \boldsymbol{x}^+)$ by combining each single instance $\boldsymbol{x}$ and its perturbation $\boldsymbol{x}^+$, we are able to use the *noise contrastive estimation* (NCE) loss [16] to learn a feature embedding $\boldsymbol{\Phi}$ from positive and negative pairs. In this paper, we focus on such a NCE loss which has the form of $\mathcal{L}_{\mathrm{NCE}}(\boldsymbol{\Phi}) = \mathbb{E}_{\boldsymbol{x}, \boldsymbol{x}_j^- \in \mathcal{X}}[-\log(\mathrm{e}^{\boldsymbol{\Phi}(\boldsymbol{x})^\top \boldsymbol{\Phi}(\boldsymbol{x}^+)} / (\mathrm{e}^{\boldsymbol{\Phi}(\boldsymbol{x})^\top \boldsymbol{\Phi}(\boldsymbol{x}^+)} + \sum_{j=1}^n \mathrm{e}^{\boldsymbol{\Phi}(\boldsymbol{x})^\top \boldsymbol{\Phi}(\boldsymbol{x}_j^-)}))]$. Here instances $\boldsymbol{x}$ and $\{\boldsymbol{x}_j^-\}_{j=1}^n$ are uniformly sampled from the training data $\mathcal{X}$, and n is the batch size.

Admittedly, as the original prototype of CL, instance discrimination is very critical to ensuring the effectiveness of most CL methods. However, the feature dimensionality settings in existing CL methods are usually very high (*e.g.*, 2048-dimension and 4096-dimension in [7, 9]), which are much larger than the feature dimensionality in most fully supervised learning methods (*e.g.*, 512-dimension and 1024-dimension in [10, 15]). We demonstrate that learning contrastive embeddings in such high-dimensional space can be weak in capturing the similarity between pairwise instances. To address this issue, in this paper, we propose a novel framework to learn contrastive embedding in low-dimensional space, which uses a *sparse / low-rank* regularized projection layer for reconstruction.

PCA & Autoencoder. As a classical unsupervised / self-supervised learning method, *principal component analysis* (PCA) has shown promising results in many machine learning tasks [39, 45, 4]. Actually, PCA shares very similar motivation with the instance discrimination of CL. It is well-known that PCA seeks for a vector $\boldsymbol{p} \in \mathbb{R}^m$ to scatter instances in the projection space by maximizing the variance $\mathbb{E}_{\boldsymbol{x} \in \mathcal{X}}[(\boldsymbol{x} - \overline{\boldsymbol{x}})^\top \boldsymbol{p} \boldsymbol{p}^\top (\boldsymbol{x} - \overline{\boldsymbol{x}})]$, where $\overline{\boldsymbol{x}} \in \mathbb{R}^m$ is the mean of all instances in the training data $\mathcal{X}$. Enlarging such a variance is quite similar to the instance discrimination of CL which also pushes away data pairs to scatter instances. PCA has another reconstruction based form $\mathbb{E}_{\boldsymbol{x} \in \mathcal{X}}[\|\boldsymbol{P} \boldsymbol{P}^\top \boldsymbol{x} - \boldsymbol{x}\|_2^2]$ which is equivalent to the variance maximization ($\boldsymbol{P} \in \mathbb{R}^{m \times l}$ is the projection matrix and $l \in \mathbb{Z}_+$ is the dimensionality of orthogonal space). To further improve the fitting ability of PCA for complex data, the non-linear extension Autoencoder introduces the non-linear activation function σ and two different projection matrices $\boldsymbol{P}$ and $\boldsymbol{P}'$ to reconstruct the training data in the by minimizing the objective $\mathbb{E}_{\boldsymbol{x} \in \mathcal{X}}[\|\sigma(\boldsymbol{P}'^\top \sigma(\boldsymbol{P}^\top \boldsymbol{x})) - \boldsymbol{x}\|_2^2]$. Some further extensions such as *masked autoencoder* (MAE) [17] achieved very promising results in several downstream tasks.

In this paper, we are inspired by PCA / Autoencoder to reduce the dimensionality of contrastive embedding based on a sparse / low-rank regularized reconstruction loss. Interestingly, from this perspective, our method can also be regarded as a *natural combination* of two main existing self-supervised learning approaches.

2 Methodology

In this section, we first investigate the distribution of instances scattered by CL in the high-dimensional feature space. After that, we propose a novel framework dubbed contrastive learning with low-dimensional reconstruction by introducing a new sparse projection layer. The learning objective and the corresponding optimization algorithm are finally designed with convergence guarantee.

2.1 Motivation

As we mentioned before, the contrastive embedding $\boldsymbol{\Phi}$ maps an m-dimensional instance into the H-dimensional feature space. Now we want to investigate the distribution of data points in such an H-dimensional space. We consider the H-dimensional *hypercube* and its *inscribed-suprasphere*. We suppose that the edge length of the H-dimensional hypercube is $2r$, and the radius of its inscribed-

suprasphere will be r. Then their corresponding volumes in the high-dimensional space are

$$\mathcal{V}_{\text{cube}}(H) = (2r)^H \qquad \text{and} \qquad \mathcal{V}_{\text{sphere}}(H) = (2r^H \pi^{H/2})/(H \cdot \Gamma(H/2)), \qquad (2)$$

respectively, where $\Gamma(\cdot)$ is the gamma function [37] having a form of $\Gamma(z) = \int_0^\infty t^{z-1} e^{-t} dt$. We further study the ratio of the suprasphere volume to the hypercube volume. We let $H \to \infty$ and the formulation $\lim_{H \to \infty} \mathcal{V}_{\text{sphere}}(H)/\mathcal{V}_{\text{cube}}(H)$ equals to

$$\lim_{H \to \infty} (\pi^{H/2}/(H \cdot \Gamma(H/2)))/2^{H-1} \leq \lim_{H \to \infty} \pi^{(H-1)/2}/2^{H-1} = \lim_{H \to \infty} (\pi/4)^{(H-1)/2} = 0, \quad (3)$$

and thus we have $\lim_{H \to \infty} \mathcal{V}_{\text{sphere}}(H)/\mathcal{V}_{\text{cube}}(H) = 0$ by using the fact that $\mathcal{V}_{\text{sphere}}(H)/\mathcal{V}_{\text{cube}}(H) \geq 0$. This result of volume ratio clearly reveals that the proportion of the inscribed-suprasphere in the hypercube will gradually converge to 0 with the increase of the dimensionality H. It means that, in the high-dimensional hypercube, a random given data point is less likely to appear *inside* of the inscribed-suprasphere (*i.e.*, in the *central area* of the hypercube) but it will usually exist *outside* of the inscribed-suprasphere (*i.e.*, in the *corner area* of the hypercube).

However, the learning objective of CL expects to scatter all instances in the H-dimensional hypercube, and thus making the N instances *sparsely distribute* in the $\widehat{N} = 2^H$ corners. Specifically, for the common dimensionality setting $H = 2048$ in popular CL methods, we have that

$$\widehat{N} = 2^H = 2^{2048} = 16^{512} \gg 10^{512} \gg 10^6 = N, \qquad (4)$$

which implies that the corner number $\widehat{N}$ is *significantly larger* than the sample number N. In this case, the distribution of instances in the feature space will be very sparse, and all instances are far away from each other. Thereby the learning algorithm can hardly capture the intrinsic similarity between intra-class instances, and the downstream recognition tasks will be affected.

To be more religious, we consider the *min-max distance ratio* to investigate the *distance contrast* in the high-dimensional space. For the *independent and identically distributed* (i.i.d.) instances $\boldsymbol{x}$, $\boldsymbol{x}_i \in \mathbb{R}^m$ $(i = 1, 2, \ldots, n)$, their embeddings $\boldsymbol{\Phi}(\boldsymbol{x})$ and $\boldsymbol{\Phi}(\boldsymbol{x}_i)$ are also i.i.d. no matter how the embedding is learned [13]. The following Theorem 1 reveals that the minimal distance $\mathcal{D}_{\boldsymbol{\Phi}}^{\min}(H)$ and the maximal distance $\mathcal{D}_{\boldsymbol{\Phi}}^{\max}(H)$ tend to be equivalent in the high-dimensional space [1] (provided that $\boldsymbol{\Phi}(\boldsymbol{x})$ and $\boldsymbol{\Phi}(\boldsymbol{x}_i)$ are

Figure 2: Distance distributions of contrastive embeddings learned on *STL-10* with different feature dimensionalities 256, 512, and 2048.

i.i.d. to each other), so the similarity between pairwise instances can hardly provide contrast to discriminate the intra-class and inter-class (as shown by the distance distributions in Fig. 2).

Theorem 1. *For any given i.i.d. random data points $\boldsymbol{x}$, $\boldsymbol{x}_1$, $\boldsymbol{x}_2$, $\ldots$, $\boldsymbol{x}_n \in \mathbb{R}^m$, we denote $\mathcal{D}_{\boldsymbol{\Phi}}^{\max}(H) = \max\{\mathcal{D}_{\boldsymbol{\Phi}}(\boldsymbol{x}, \boldsymbol{x}_i)|i = 1, \ldots, n\}$ and $\mathcal{D}_{\boldsymbol{\Phi}}^{\min}(H) = \min\{\mathcal{D}_{\boldsymbol{\Phi}}(\boldsymbol{x}, \boldsymbol{x}_i)|i = 1, \ldots, n\}$. Then we have that $\lim_{H \to \infty}\{\text{var}[\mathcal{D}_{\boldsymbol{\Phi}}(\boldsymbol{x}, \boldsymbol{x}_i)/\mathbb{E}(\mathcal{D}_{\boldsymbol{\Phi}}(\boldsymbol{x}, \boldsymbol{x}_i))]\} = 0$ and*

$$\mathcal{P}\left\{\lim_{H \to \infty} (\mathcal{D}_{\boldsymbol{\Phi}}^{\max}(H) - \mathcal{D}_{\boldsymbol{\Phi}}^{\min}(H))/\mathcal{D}_{\boldsymbol{\Phi}}^{\min}(H) = 0\right\} = 1, \qquad (5)$$

where the distance function $\mathcal{D}_{\boldsymbol{\Phi}}(\cdot, \cdot)$ is defined in Eq. (1) and the feature embedding $\boldsymbol{\Phi}$ is learned from the training data and independent to the data points $\boldsymbol{x}$, $\boldsymbol{x}_1$, $\boldsymbol{x}_2$, $\ldots$, $\boldsymbol{x}_n$.

In summary, from the above analytical results, we can clearly find that it is very necessary to constrain the dimensionality of existing CL approaches in a reasonable range. Motivated by this, in the next subsection, we provide the formulation of our proposed framework CLLR which reduces the dimensionality of contrastive embedding by a sparse projection layer.

2.2 Formulation

As we discussed in the previous subsection, the feature embedding $\boldsymbol{\Phi}$ transforms the raw data from m-dimensional space into H-dimensional space, where $\boldsymbol{\Phi}$ is learned by the NCE loss. To avoid high-dimensional features, we may directly reduce the dimensionlaity of the output layer, but this will cause the dimensional collapse with insufficient instance discrimination (as we discussed in
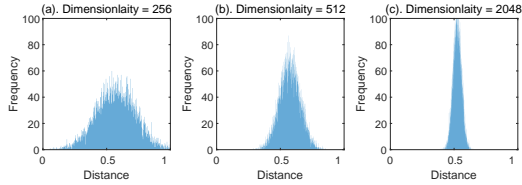
Section 1). Thereby, we consider to use an additional matrix $L \in \mathbb{R}^{H \times H}$ to transform the feature embedding result $\boldsymbol{\Phi}(\boldsymbol{x})$ into the latent vector $L \cdot \boldsymbol{\Phi}(\boldsymbol{x})$, and then we minimize $\|L^{\top} L \cdot \boldsymbol{\Phi}(\boldsymbol{x}) - \boldsymbol{\Phi}(\boldsymbol{x})\|_2^2$, encouraging the latent vector to preserve the useful information in $\boldsymbol{\Phi}(\boldsymbol{x})$. When we further introduce the low-rank constraint for L, we can obtain a low-dimensional latent space for contrastive learning.

$\ell_{2,1}$-**Norm based Regularization.** The row (column) sparsity is a long-standing concept which aims to maintain very few non-zero columns for a matrix. When we employ the well-known $\ell_{2,1}$-norm to restrict the projection matrix L, we can certainly have a column-sparse L which selects the important features in $\boldsymbol{\Phi}(\boldsymbol{x}) \in \mathbb{R}^H$ corresponding to the non-zero columns. Then we use the selected features to reconstruct the original feature embedding, *i.e.*,

$$\mathcal{R}_{2,1}(\boldsymbol{\Phi}, L) = \mathbb{E}_{\boldsymbol{x} \in \mathcal{X}}[\|L^{\top} L \cdot \boldsymbol{\Phi}(\boldsymbol{x}) - \boldsymbol{\Phi}(\boldsymbol{x})\|_2^2] + \alpha \|L\|_{2,1}, \tag{6}$$

where $L \in \mathbb{R}^{H \times H}$ and $\alpha > 0$ is tuned by users. Note that the column sparsity is just a special case of the low-rank, but considering its good usability, here we can easily obtain a low-dimensional feature embedding $L \cdot \boldsymbol{\Phi}(\boldsymbol{x})$ if the above L is column sparse. We also provide the following nuclear-norm based formulation to consider the more general case of low-dimensional space.

Nuclear-Norm based Regularization. To ensure the projection result $L \cdot \boldsymbol{\Phi}(\boldsymbol{x})$ in a low-dimensional space, a more general way is directly restricting the projection matrix L to be low-rank. Then, the column vectors of L will be linearly dependent so that we can remove the redundant column to achieve a low-dimensional projection space. The realized formulation can be written as

$$\mathcal{R}_{\text{nuclear}}(\boldsymbol{\Phi}, L) = \mathbb{E}_{\boldsymbol{x} \in \mathcal{X}}[\|L^{\top} L \cdot \boldsymbol{\Phi}(\boldsymbol{x}) - \boldsymbol{\Phi}(\boldsymbol{x})\|_2^2] + \alpha \|L\|_*, \tag{7}$$

where $L \in \mathbb{R}^{H \times H}$ and $\alpha > 0$ is tuned by users. When we obtain the learned projection matrix L^*, we need to further compute its *maximal linearly independent set* $\mathcal{A}$, and then we calculate the final projection matrix $\widehat{L} \in \mathbb{R}^{H \times H}$ by setting [1] the redundant columns of L^* to $\mathbf{0}$.

For the above two different formulations in Eq. (6) and Eq. (7), it is hard to say which one is theoretically better. Actually, their final performance may also be influenced by the non-convexity of the learning objectives. Therefore, in our experiments, we evaluate both the two regularizations on multiple domains. Now we want to summarize our final learning objective as follows.

Learning Objective of CLLR. Based on the realized formulation in Eq. (6) and Eq. (7), we can easily deploy the proposed two regularizers in the learning objective of conventional CL methods. Without loss of generality, for most existing CL methods equipped with NCE loss, we build the following framework of contrastive learning with low-dimensional reconstruction (CLLR)

$$\min_{\boldsymbol{\Phi} \in \mathcal{H}, L \in \mathbb{R}^{H \times H}} \{\mathcal{F}(\boldsymbol{\Phi}, L) = \mathcal{L}_{\text{NCE}}(\boldsymbol{\Phi}) + \lambda \mathcal{R}(\boldsymbol{\Phi}, L)\}, \tag{8}$$

where the regularization parameter $\lambda > 0$ is tuned by users and the regularizer $\mathcal{R}(\boldsymbol{\Phi}, L)$ can be realized by $\mathcal{R}_{2,1}(\boldsymbol{\Phi}, L)$ and $\mathcal{R}_{\text{nuclear}}(\boldsymbol{\Phi}, L)$ in Eq. (6) and Eq. (7), respectively. As a regularized learning objective, CLLR is very generic because here the loss term $\mathcal{L}_{\text{NCE}}(\boldsymbol{\Phi})$ can be implemented by many existing CL methods. In the next subsection, we provide iteration algorithm to solve Eq. (8).

2.3 Optimization

Minimizing the objective function in Eq. (8) is a typical batch optimization problem [48], where both the loss function $\mathcal{L}_{\text{NCE}}(\boldsymbol{\Phi})$ and the regularizer $\mathcal{R}(\boldsymbol{\Phi}, L)$ involve all training data. Therefore, we adopt the *stochastic gradient descent* (SGD) method [22] to solve it, and here we demonstrate the stochastic gradient for the objective function $\mathcal{F}(\boldsymbol{\Phi}, L)$. Specifically, for $n + 1$ (*i.e.*, the batch size) randomly selected data points $\{\boldsymbol{x}_{b_j} | \boldsymbol{x}_{b_j} \in \mathcal{X}, b_j \in B\}_{j=1}^{n+1}$, the NCE loss already has a stochastic form [2], so here we need to demonstrate the stochastic loss for the regularizer in the mini-batch, *i.e.*,

$$\mathcal{R}_B(\boldsymbol{\Phi}, L) = [1/(n+1)] \sum_{i=1}^{n+1} \|L^{\top} L \cdot \boldsymbol{\Phi}(\boldsymbol{x}_{b_i}) - \boldsymbol{\Phi}(\boldsymbol{x}_{b_i})\|_2^2 + \alpha \widehat{\mathcal{R}}(L), \tag{10}$$

---

[1] Here the i-column of $\widehat{L}$ is $\widehat{L}_i = L_i^*$ if $L_i^* \in \mathcal{A}$ and $\widehat{L}_i = \mathbf{0}$ if $L_i^* \notin \mathcal{A}$, in which $i = 1, 2, \ldots, H$.

[2] Here we denote NCE loss $\mathcal{L}_{\text{NCE}}(\boldsymbol{\varphi}) = \mathbb{E}[\ell(\boldsymbol{\varphi}; \{\boldsymbol{x}_{b_j}\}_{j=1}^{n+1})]$, where the function $\ell(\boldsymbol{\varphi}; \{\boldsymbol{x}_{b_j}\}_{j=1}^{n+1}) = -\log(\exp(\boldsymbol{\varphi}(\boldsymbol{x}_{b_{n+1}})^{\top} \boldsymbol{\varphi}(\boldsymbol{x}_{b_{n+1}}^+))/(\exp(\boldsymbol{\varphi}(\boldsymbol{x}_{b_{n+1}}))^{\top} \boldsymbol{\varphi}(\boldsymbol{x}_{b_{n+1}}^+)) + \sum_{j=1}^{n} \exp(\boldsymbol{\varphi}(\boldsymbol{x}_{b_j}))^{\top} \boldsymbol{\varphi}(\boldsymbol{x}_{b_j}^-))))$. The index vector set $B = \{\boldsymbol{b} = (b_1, \ldots, b_{n+1})^{\top} | b_i, b_j = 1, \ldots, N, b_i \neq b_j, i, j = 1, \ldots, n+1\}$.

Algorithm 1 Solving Eq. (8) via SGD.

Input: Training Data $\mathcal{X} = \{\boldsymbol{x}_i\}_{i=1}^N$; Step Size $\eta > 0$; Regularization Parameter $\lambda, \alpha > 0$; Batch Size $n \in \mathbb{N}_+$.

Initialize: Iteration Number $t = 0$.

For t **from** 1 **to** T**:**

    1). Uniformly pick $(n+1)$ data points $\{\boldsymbol{x}_{b_j}\}_{j=1}^{n+1}$ from $\mathcal{X}$;

    2). Compute the gradient of $f(\boldsymbol{\Phi}; \{\boldsymbol{x}_{b_j}\}_{j=1}^{n+1}) = \ell(\boldsymbol{\Phi}; \{\boldsymbol{x}_{b_j}\}_{j=1}^{n+1}) + \lambda \mathcal{R}_B(\boldsymbol{\Phi}, \boldsymbol{L}; \{\boldsymbol{x}_{b_j}\}_{j=1}^{n+1})$ via Eq. (10):

    3). Update the learning parameters:

$$\boldsymbol{\Phi}_{(t+1)} \leftarrow \boldsymbol{\Phi}_{(t)} - \eta \nabla_{\boldsymbol{\Phi}} f(\boldsymbol{\Phi}, \boldsymbol{L}; \{\boldsymbol{x}_{b_j}\}_{j=1}^{n+1}) \quad \text{and} \quad \boldsymbol{L}_{(t+1)} \leftarrow \boldsymbol{L}_{(t)} - \eta \nabla_{\boldsymbol{L}} f(\boldsymbol{\Phi}, \boldsymbol{L}; \{\boldsymbol{x}_{b_j}\}_{j=1}^{n+1}), \quad (9)$$

End.

Output: The converged $\widetilde{\boldsymbol{\Phi}}$ and $\widetilde{\boldsymbol{L}}$.

---

where $\widehat{\mathcal{R}}(\boldsymbol{L})$ indicates the penalty $\|\boldsymbol{L}\|_{2,1}$ or $\|\boldsymbol{L}\|_*$ for different regularizations. Here we use the subgradients [2] of $\ell_{2,1}$-norm and nuclear-norm for optimziation. Then the learning objective $\mathcal{F}(\boldsymbol{\Phi}, \boldsymbol{L})$ in Eq. (8) has the stochastic form $\ell(\boldsymbol{\Phi}; \{\boldsymbol{x}_{b_j}\}_{j=1}^{n+1}) + \lambda \mathcal{R}_B(\boldsymbol{\Phi}, \boldsymbol{L}; \{\boldsymbol{x}_{b_j}\}_{j=1}^{n+1})$. Based on such a stochastic loss, we further provide the SGD iteration steps in Algorithm 1 to solve Eq. (8).

In summary, introducing the projection layer (i.e., the projection matrix $\boldsymbol{L}$) merely incurs an additional stochastic gradient in Eq. (10). It means that our method can be easily implemented in most existing CL methods and only introduces very little computational overheads. In the next section, we prove that the iteration sequence $\boldsymbol{\Phi}_{(1)}, \ldots, \boldsymbol{\Phi}_{(T)}$ in Algorithm 1 converges to a stationary point of the learning objective $\mathcal{F}$ with a convergence rate $\mathcal{O}(1/\sqrt{T})$, where T is the number of iterations.

3 Theoretical Analyses

In this section, we further provide in-depth theoretical analyses for our proposed method. We investigate the convergence of learning algorithm and the lower bound of min-max distance ratio to demonstrate the effectiveness of our method. All proofs are given in *supplementary materials*.

3.1 Convergence Analysis

As we described before, the learning objective of CLLR is a regularized empirical loss which is different from the traditional empirical loss solved by SGD, so here we provide careful convergence analysis for the SGD based iterations, *i.e.*, the Algorithm 1. Specifically, we suppose the learning objective has δ-bounded gradient, and then we have the following Theorem 2.

Theorem 2. *If the function $\mathcal{F}(\boldsymbol{\Phi}, \boldsymbol{L})$ has δ-bounded gradient (i.e., $\|\nabla \mathcal{F}(\boldsymbol{\Phi}, \boldsymbol{L})\|_2 < \delta$), then we let $\eta = \sqrt{2(\mathcal{F}(\boldsymbol{\Phi}_{(0)}, \boldsymbol{L}_{(0)}) - \mathcal{F}(\boldsymbol{\Phi}^*, \boldsymbol{L}^*))/(S\delta^2 T)}$, and for the iterations in Algorithm 1 we have that*

$$\min_{0 \le t \le T-1} \mathbb{E}[\|\nabla \mathcal{F}(\boldsymbol{\Phi}_{(t)}, \boldsymbol{L}_{(t)})\|_2] \le \sqrt{2S(\mathcal{F}(\boldsymbol{\Phi}_{(0)}, \boldsymbol{L}_{(0)}) - \mathcal{F}(\boldsymbol{\Phi}^*, \boldsymbol{L}^*))/T} \delta, \qquad (11)$$

where $S > 0$ is a lipschitz constant such that $\|\nabla \mathcal{F}(\boldsymbol{\Phi}, \boldsymbol{L}) - \nabla \mathcal{F}(\boldsymbol{\Phi}', \boldsymbol{L}')\|_2 \le S \|[\boldsymbol{\Phi}, \boldsymbol{L}] - [\boldsymbol{\Phi}', \boldsymbol{L}']\|_2$.

The above Eq. (11) clearly reveals that the iteration results in Algorithm 1 can gradually converge to a stationary point with a convergence rate $\mathcal{O}(1/\sqrt{T})$ when setting the proper learning rate η and increasing the iteration number T. Therefore, the convergence of our learning algorithm is guaranteed though the additional projection layer and regularization term are introduced.

3.2 Lower Bound of Min-Max Distance Ratio

Now, we further analyze the distance between pairwise instances in the low-dimensional space. As we mentioned before, in the high-dimensional space, the min-max distance ratio trends to be 0 and thus the distance function will lose its discriminatory. Therefore, we want to investigate the value of min-max distance ratio in low-dimensional feature space learned by our method.

Our method explicitly constrain the dimensionality of the feature space, so it is intuitive that the min-max distance ratio $(\mathcal{D}_{\boldsymbol{\Phi}}^{\max}(H) - \mathcal{D}_{\boldsymbol{\Phi}}^{\min}(H))/\mathcal{D}_{\boldsymbol{\Phi}}^{\min}(H)$ in Eq. (5) should certainly be lower-bounded. To be religious, we have the following Theorem 3 to reveal the lower bound of distance ratio.

Theorem 3. *For any given $n+1$ i.i.d. random data points $\boldsymbol{x}, \boldsymbol{x}_1, \boldsymbol{x}_2, \ldots, \boldsymbol{x}_n \in \mathbb{R}^m$, we denote that $\mathcal{D}_{\widehat{\boldsymbol{\Phi}},\widehat{\boldsymbol{L}}}^{\max} = \max\{\mathcal{D}_{\widehat{\boldsymbol{\Phi}},\widehat{\boldsymbol{L}}}(\boldsymbol{x}, \boldsymbol{x}_i)|i=1,2,\ldots,n\}$ and $\mathcal{D}_{\widehat{\boldsymbol{\Phi}},\widehat{\boldsymbol{L}}}^{\min} = \min\{\mathcal{D}_{\widehat{\boldsymbol{\Phi}},\widehat{\boldsymbol{L}}}(\boldsymbol{x}, \boldsymbol{x}_i)|i=1,2,\ldots,n\}$, and then we have that*

$$\mathcal{P}\left\{(\mathcal{D}_{\widehat{\boldsymbol{\Phi}},\widehat{\boldsymbol{L}}}^{\max} - \mathcal{D}_{\widehat{\boldsymbol{\Phi}},\widehat{\boldsymbol{L}}}^{\min})/\mathcal{D}_{\widehat{\boldsymbol{\Phi}},\widehat{\boldsymbol{L}}}^{\min} \geq \alpha\lambda C(\mathcal{X})\right\} = 1, \tag{12}$$

where $\mathcal{D}_{\widehat{\boldsymbol{\Phi}},\widehat{\boldsymbol{L}}}(\boldsymbol{x}, \boldsymbol{x}_i) = \|\widehat{\boldsymbol{L}}\widehat{\boldsymbol{\Phi}}(\boldsymbol{x}) - \widehat{\boldsymbol{L}}\widehat{\boldsymbol{\Phi}}(\boldsymbol{x}_i)\|_2/rank(\widehat{\boldsymbol{L}})$, and $\widehat{\boldsymbol{\Phi}}$ and $\widehat{\boldsymbol{L}}$ are learned from Eq. (8).

From the above Eq. (12), we can easily observe that the min-max distance ratio has an explicit lower bound which is mainly determined by the two regularization parameters α and λ (given the training data $\mathcal{X}$). It means that the low-rank reconstruction terms (*i.e.*, Eq. (6) and Eq. (7)) make the min-max distance ratio be controllable, and the larger regularization parameters can produce the better lower bound. When the min-max distance ratio is lower-bounded, our CLLR predicts low similarities for inter-cluster and high similarities for intra-cluster, so that the learned embedding effectively captures the intrinsic similarities / features and thus improving the performance of downstream tasks.

4 Experimental Results

In this section, we show experimental results on real-world datasets to validate the effectiveness of our proposed method. In detail, we first conduct ablation study to reveal the usefulness of our introduced new block and new regularizers. Then, we compare our proposed learning algorithm with existing state-of-the-art models on vision and language tasks. Finally, we test our method on the CL based reinforcement learning task. Further experiments such as parametric sensitivity and running time comparison are given in *supplementary materials*. The training process is implemented on Pytorch [29] with NVIDIA TeslaV100 GPUs. We adopt the projection result $\boldsymbol{L}\boldsymbol{\Phi}(\boldsymbol{x})$ for feature extraction, where regularization parameters λ and α are fixed to 0.1 and 10, resepectively. The hyper-parameters of compared methods are set to the recommended values according to their original papers.

4.1 Ablation Study

In this subsection, we conduct ablation study on the superiority of the low-dimensional contrastive embedding (*i.e.*, our method) over the traditional contrastive embedding (*i.e.*, the baseline method). We use the *STL-10* and *CIFAR-10* datasets to train the baseline *SimCLR* [7] and two implementations of CLLR, *i.e.*, the $\ell_{2,1}$-norm based regularization and nuclear-norm based regularization. We train all models with 100 and 400 epochs with the

Table 1: Classification accuracy rates (mean $\pm$ std) of high-dimensional embedding and low-dimensional embedding on *STL-10* and *CIFAR-10* datasets (negative sample size = 256).

METHOD	STL-10		CIFAR-10	
	epochs=100	epochs=400	epochs=100	epochs=400
4096-dim. (w/o $\mathcal{R}(\boldsymbol{\Phi}, \boldsymbol{L})$)	55.1 ± 1.1	75.2 ± 3.1	65.1 ± 1.9	85.4 ± 4.2
3072-dim. (w/o $\mathcal{R}(\boldsymbol{\Phi}, \boldsymbol{L})$)	54.4 ± 3.1	75.2 ± 2.1	67.2 ± 3.5	86.9 ± 6.1
2048-dim. (w/o $\mathcal{R}(\boldsymbol{\Phi}, \boldsymbol{L})$)	56.3 ± 2.1	76.2 ± 1.1	66.3 ± 3.1	89.3 ± 2.1
512-dim. (w/o $\mathcal{R}(\boldsymbol{\Phi}, \boldsymbol{L})$)	56.4 ± 2.5	75.2 ± 0.1	66.4 ± 5.1	90.3 ± 0.6
256-dim. (w/o $\mathcal{R}(\boldsymbol{\Phi}, \boldsymbol{L})$)	55.3 ± 4.1	74.2 ± 2.1	64.3 ± 5.1	88.3 ± 3.1
512-dim. (w/o sparity, $\alpha = 0$)	$\mathbf{56.5 \pm 2.5}$	75.5 ± 0.5	66.2 ± 4.9	90.1 ± 1.2
256-dim. (w/o sparity, $\alpha = 0$)	55.9 ± 2.1	74.1 ± 2.3	64.7 ± 2.1	88.4 ± 2.6
512-dim. (w / $\ell_{2,1}$-norm)	$56.3 \pm 8.2 -$	$78.3 \pm 0.5 \checkmark$	$\mathbf{67.5 \pm 0.2} -$	$\mathbf{92.5 \pm 0.2} \checkmark$
512-dim. (w / nuclear-norm)	$56.2 \pm 3.2 -$	$\mathbf{79.2 \pm 0.2} \checkmark$	$67.5 \pm 2.5 -$	$92.5 \pm 2.3 \checkmark$
256-dim. (w / $\ell_{2,1}$-norm)	$56.2 \pm 1.2 -$	$\mathbf{79.3 \pm 0.5} \checkmark$	$65.5 \pm 0.5 -$	$92.3 \pm 0.3 \checkmark$
256-dim. (w / nuclear-norm)	$56.3 \pm 3.2 -$	$79.2 \pm 0.2 \checkmark$	$65.2 \pm 5.5 -$	$\mathbf{93.1 \pm 1.3} \checkmark$

same batch size and learning rate, respectively, and we record the test accuracy of all methods by fine-tuning a linear *softmax*. The baseline method learns contrastive embeddings in the high-dimensional space (dimension = 2048, 3072, and 4096) and the simply fixed low-dimensional space (dimension = 256 and 512). We also include the baseline results that do not use the $\ell_{2,1}$-norm and nuclear norm constraints (*i.e.*, $\alpha = 0$). Our method learns embeddings in low-dimensional space, where we use the regularizer to maintain the corresponding non-zero columns in the projection matrix $\boldsymbol{L}$.

We record the test accuracy (mean $\pm$ std, 5 random trials) of compared methods at the 100-*th* epoch and 400-*th* epoch in Tab. 1. We can observe that the baseline method is better than our method in the first 100 epochs, but the two implementations of our method can outperform the baseline method with the increase of iterations. This is because that the baseline method only emphasizes on the instance discrimination, so it can quickly discriminate the training data in the early epochs. However, in the latter epochs, the low-rank reconstruction in our method becomes useful in capturing the similarity between pairwise instances. Meanwhile, we can find that the average accuracy of nuclear-norm based
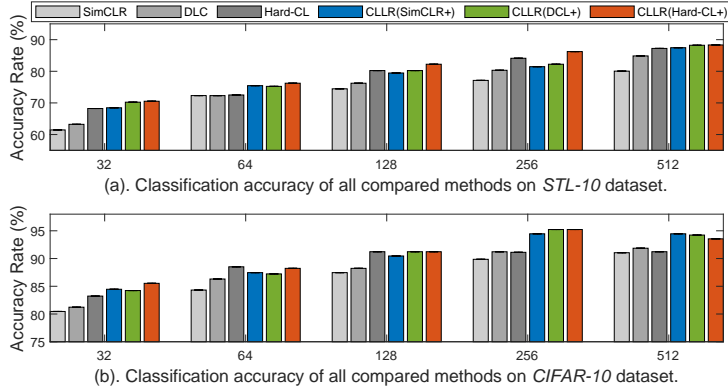
Figure 4: Classification accuracy of all methods on *STL-10* and *CIFAR-10* datasets. The negative sample size is from 32 to 512.

regularization is slightly higher than the $\ell_{2,1}$-norm based one on both two datasets. Furthermore, we also perform the t-test at significance level 0.05 in the last column, and "✓" indicates that our method is significantly better than the best baseline result. In our following experiments, we employ the 256-dimensional latent features for multiple domain tasks.

4.2 Experiments on Sentence Representation

In this subsection, we employ the *BookCorpus* dataset [23] to evaluate the performance of all compared methods on six text classification tasks, including movie review sentiment (*MR*), product reviews (*CR*), subjectivity classification (*SUBJ*), opinion polarity (*MPQA*), question type classification (*TREC*), and paraphrase identification (*MSRP*). We follow the experimental settings in the baseline method *quick-thought* (QT) [26], which chooses the neighboring sentences as positive pairs. Here the 10-fold cross validation is adopted, and the average classification accuracy is listed in Tab. 2.

For the six classification tasks, our method improves the classification accuracy of baseline method QT for at least one percentage on most classification benchmarks. The distance histograms of QT, *debiased contrastive learning* (DCL) [11], *hard negative based contrastive learning* (HCL) [30], and our CLRR are

Table 2: Classification accuracy (%) of all methods on *Book-Corpus* dataset including six text classification tasks.

METHOD	MR	CR	SUBJ	MPQA	TREC	MSRP
QT[26]	76.8	81.3	86.6	93.4	89.8	73.6
DCL[11]	76.2	82.9	86.9	93.7	89.1	74.7
HCL[30]	77.4	83.6	86.8	93.4	88.7	73.5
CLLR(DCL+$\ell_{2,1}$-norm)	77.9	83.3	**87.9**	93.7	**91.3**	75.2
CLLR(DCL+nuclear-norm)	**78.2**	**83.7**	87.2	**95.8**	91.2	**75.7**

shown in Fig. 3. We clearly observe that our method obtains the more accurate distance determination than baseline methods, and this reveals that our method is effective for the text classification task.

4.3 Experiments on Image Classification

In this subsection, we validate the effectiveness of our method on the image classification task. Here we select *contrastive multiview coding* (CMC) [35] as baseline methods, and implement our method CLLR under such a classical framework. We also compare our method with three additional state-of-the-art methods including DCL, HCL, SwAV [3], and CO2 [38] on *STL-10* [12], *CIFAR-10* [24], and *ImageNet-100* [31] datasets. All methods are fairly implemented by the *ResNet50* with the same training epoch 100.

For *STL-10* and *CIFAR-10* datasets, we record the classification accuracy of all compared methods with varying numbers of negative sample.
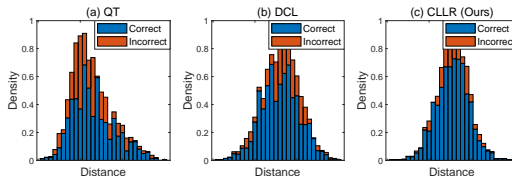

Figure 3: Distance histograms obtained by different methods (QT, DCL, and our proposed CLRR) on *Book-Corpus* dataset. The proportion of incorrect prediction of CLLR is clearly lower than the compared methods.

From Fig. 4, we can clearly observe that our method CLLR successfully improves the baseline for at least 1% and 2% on *CIFAR-10*

8

dataset and *STL-10* dataset, respectively. Similar experiments are conducted on *ImageNet-100* dataset, and Tab. 3 shows that our method consistently improves all baseline methods, where our method improves the baseline CMC from 73.58% to 76.91%. For different negative sample sizes, the accuracy rates of our method are also higher than all compared methods, and it clearly demonstrates the effectiveness of our method. Since CLLR is implemented on different baselines, our method has good compatibility with existing CL algorithms on the image classification task. In *supplementary materials*, we further compare our method with the distillation based CL models [5, 47] (*i.e.*, the low-dimensional small networks supervised by the original contrastive embeddings), and the results clearly demonstrate the superiority of our method.

4.4 Experiments on Reinforcement Learning

This subsection further extends our experiments on reinforcement learning task, which is another application scenario of contrastive learning. Here the *contrastive unsupervised representations for reinforcement learning* (CURL) [25] method is employed to perform image-based policy control on representation learned by the CL algorithm. All methods are tested on the DeepMind control suite [34], which consists of six control tasks listed in Tab. 4. By following the experimental settings in CURL, the positive pair is built by simply cropping a single image, and the negative pair is composed of each two images in the control sequence. All methods are retrained for 3 times, and the corresponding means and standards of 100K scores are shown in Tab. 4.

Table 3: Classification accuracy (%) of all methods on *ImageNet-100* dataset with negative sample size 1024 and 4096.

METHOD	1024		4096	
	Top1	Top5	Top1	Top5
CMC[35]	60.23	79.23	73.58	92.06
SwAV[3]	60.93	79.43	75.78	92.86
DCL[11]	61.01	78.99	74.60	92.08
HCL[30]	60.89	79.33	74.66	92.32
CO2[38]	61.21	79.32	73.96	93.02
CLLR(CMC+$\ell_{2,1}$-norm)	62.03	80.64	75.97	94.22
CLLR(CMC+nuclear-norm)	61.23	80.50	**76.91**	94.03
CLLR(HCL+$\ell_{2,1}$-norm)	61.29	**81.10**	76.88	94.19
CLLR(HCL+nuclear-norm)	**62.43**	80.98	76.89	**94.25**

For the six control tasks, our method consistently outperforms the baseline method CURL with higher means. When compared to DCL and HCL methods, our method almost achieves the best results in all six scenarios. Although our method CLRR (CURL+nuclear-norm) has slightly lower scores than CURL or DCL on the *Run / Walk* tasks, our method shows smaller variance. Moreover, when

Table 4: 100K Scores (mean $\pm$ std, 3 random trials) achieved by all methods on the six control tasks.

METHOD	*Spin*	*Swingup*	*Easy*	*Run*	*Walk*	*Catch*
CURL[25]	413±53	680±32	908±86	**298±38**	621±121	826±42
DCL[11]	422±23	672±52	878±96	248±98	**626±98**	836±12
HCL[30]	420±61	678±82	869±116	268±42	623±26	819±62
CLLR(CURL+)	**424±53**	683±23	**925±33**	296±32	625±23	843±17
CLLR(DCL+)	423±13	**684±83**	919±57	287±67	625±33	**844±27**
CLLR(HCL+)	422±41	681±13	911±85	292±78	**626±59**	839±33

we incorporate our method to DCL and HCL, our method could further improve the overall scores of compared methods on the six tasks. This also reveals that our method is compatible with existing CL algorithms on the reinforcement learning task.

5 Conclusion and Future Work

In this paper, we considered the issue of high-dimensional features existing in the current contrastive learning method. To overcome such an issue, we proposed a novel framework called contrastive learning with low-dimensional reconstruction (CLLR), which uses a sparse projection layer to reduce the dimensionality of the feature embedding. We reconstructed the original high-dimensional features in the low-dimensional projection space while preserving the basic objective for instance discrimination, and thus successfully learning low-dimensional contrastive embeddings. To the best of our knowledge, this is the first work in CL that considers reducing the feature dimensionality. We conducted intensive theoretical analyses to guarantee the effectiveness of our method. Comparison experiments on real-world datasets across multiple domains indicated that our learning algorithm acquires more reliable feature embedding than state-of-the-art methods. Both the theoretical and experimental results clearly demonstrated the necessity / significance of learning low-dimensional contrastive embeddings. Our approach mainly focuses on the mainstream CL models which use both positive and negative pairs. The effectiveness of negative-free CL has also been shown by recent works such as BYOL and SimSiam. When the negative pairs are unavailable, exploring the corresponding optimal (low-dimensional) projection space would be interesting future work.

References

[1] Kevin Beyer, Jonathan Goldstein, Raghu Ramakrishnan, and Uri Shaft. When is "nearest neighbor" meaningful? In *International conference on database theory*, pages 217–235. Springer, 1999. 2.1

[2] Stephen Boyd, Stephen P Boyd, and Lieven Vandenberghe. *Convex optimization*. Cambridge university press, 2004. 2.3

[3] Mathilde Caron, Ishan Misra, Julien Mairal, Priya Goyal, Piotr Bojanowski, and Armand Joulin. Unsupervised learning of visual features by contrasting cluster assignments. In *Advances in neural information processing systems (NeurIPS)*, pages 1401–1413, 2020. 1, 4.3, 3

[4] Ines Chami, Albert Gu, Dat P Nguyen, and Christopher Ré. Horopca: Hyperbolic dimensionality reduction via horospherical projections. In *International Conference on Machine Learning (ICML)*, pages 1419–1429, 2021. 1.1

[5] Liqun Chen, Dong Wang, Zhe Gan, Jingjing Liu, Ricardo Henao, and Lawrence Carin. Wasserstein contrastive representation distillation. In *IEEE Conference on Computer Vision and Pattern Recognition (CVPR)*, pages 16296–16305, 2021. 1, 4.3

[6] Shuo Chen, Gang Niu, Chen Gong, Jun Li, Jian Yang, and Masashi Sugiyama. Large-margin contrastive learning with distance polarization regularizer. In *International Conference on Machine Learning (ICML)*, pages 1673–1683, 2021. 1

[7] Ting Chen, Simon Kornblith, Mohammad Norouzi, and Geoffrey Hinton. A simple framework for contrastive learning of visual representations. In *International Conference on Machine Learning (ICML)*, pages 1597–1607, 2020. 1, 1.1, 4.1

[8] Xuxi Chen, Wuyang Chen, Tianlong Chen, Ye Yuan, Chen Gong, Kewei Chen, and Zhangyang Wang. Self-pu: Self boosted and calibrated positive-unlabeled training. In *International Conference on Machine Learning (ICML)*, pages 1510–1519, 2020. 1

[9] Anoop Cherian and Shuchin Aeron. Representation learning via adversarially-contrastive optimal transport. In *International Conference on Machine Learning (ICML)*, pages 1820–1830, 2020. 1, 1.1

[10] Xu Chu, Yang Lin, Yasha Wang, Xiting Wang, Hailong Yu, Xin Gao, and Qi Tong. Distance metric learning with joint representation diversification. In *International Conference on Machine Learning (ICML)*, pages 1962–1973, 2020. 1, 1.1

[11] Ching-Yao Chuang, Joshua Robinson, Lin Yen-Chen, Antonio Torralba, and Stefanie Jegelka. Debiased contrastive learning. *Advances in Neural Information Processing Systems (NeurIPS)*, 33, 2020. 1, 2, 4.2, 3, 4

[12] Adam Coates, Andrew Ng, and Honglak Lee. An analysis of single-layer networks in unsupervised feature learning. In *International conference on artificial intelligence and statistics (AISTATS)*, pages 215–223, 2011. 4.3

[13] Shib Dasgupta, Michael Boratko, Dongxu Zhang, Luke Vilnis, Xiang Li, and Andrew McCallum. Improving local identifiability in probabilistic box embeddings. *Advances in Neural Information Processing Systems (NeurIPS)*, 33:182–192, 2020. 2.1

[14] Alexey Dosovitskiy, Jost Tobias Springenberg, Martin Riedmiller, and Thomas Brox. Discriminative unsupervised feature learning with convolutional neural networks. In *Advances in neural information processing systems (NeurIPS)*, volume 27, pages 766–774, 2014. 1, 1.1

[15] Jason Xiaotian Dou, Lei Luo, and Raymond Mingrui Yang. An optimal transport approach to deep metric learning (student abstract). In *Proceedings of the AAAI Conference on Artificial Intelligence (AAAI)*, volume 36, pages 12935–12936, 2022. 1.1

[16] Michael Gutmann and Aapo Hyvärinen. Noise-contrastive estimation: A new estimation principle for unnormalized statistical models. In *International Conference on Artificial Intelligence and Statistics (AISTATS)*, pages 297–304, 2010. 1.1

[17] Kaiming He, Xinlei Chen, Saining Xie, Yanghao Li, Piotr Dollár, and Ross Girshick. Masked autoencoders are scalable vision learners. *arXiv preprint arXiv:2111.06377*, 2021. 1.1

[18] Gordon Hughes. On the mean accuracy of statistical pattern recognizers. *IEEE transactions on information theory*, 14(1):55–63, 1968. 1

[19] Ziyu Jiang, Tianlong Chen, Bobak Mortazavi, and Zhangyang Wang. Self-damaging contrastive learning. In *International Conference on Machine Learning (ICML)*, 2021. 1

[20] Li Jing, Pascal Vincent, Yann LeCun, and Yuandong Tian. Understanding dimensional collapse in contrastive self-supervised learning. *arXiv preprint arXiv:2110.09348*, 2021. 1, 1.1

[21] Longlong Jing and Yingli Tian. Self-supervised visual feature learning with deep neural networks: A survey. *IEEE Transactions on Pattern Analysis and Machine Intelligence*, 2020. 1

[22] Rie Johnson and Tong Zhang. Accelerating stochastic gradient descent using predictive variance reduction. *Advances in neural information processing systems (NeurIPS)*, 26:315–323, 2013. 2.3

[23] Ryan Kiros, Yukun Zhu, Russ R Salakhutdinov, Richard Zemel, Raquel Urtasun, Antonio Torralba, and Sanja Fidler. Skip thought vectors. *Advances in neural information processing systems (NeurIPS)*, 28:3294–3302, 2015. 4.2

[24] Alex Krizhevsky, Geoffrey Hinton, et al. Learning multiple layers of features from tiny images. 2009. 4.3

[25] Michael Laskin, Aravind Srinivas, and Pieter Abbeel. Curl: Contrastive unsupervised representations for reinforcement learning. In *International Conference on Machine Learning (ICML)*, pages 5639–5650, 2020. 4.4, 4

[26] Lajanugen Logeswaran and Honglak Lee. An efficient framework for learning sentence representations. In *International Conference on Learning Representations (ICLR)*, 2018. 4.2, 2

[27] Gang Niu, Marthinus Christoffel du Plessis, Tomoya Sakai, Yao Ma, and Masashi Sugiyama. Theoretical comparisons of positive-unlabeled learning against positive-negative learning. In *Advances in neural information processing systems (NeurIPS)*, pages 1199–1207, 2016. 1

[28] Aaron van den Oord, Yazhe Li, and Oriol Vinyals. Representation learning with contrastive predictive coding. *arXiv preprint arXiv:1807.03748*, 2018. 1

[29] Adam Paszke, Sam Gross, Francisco Massa, Adam Lerer, James Bradbury, Gregory Chanan, Trevor Killeen, Zeming Lin, Natalia Gimelshein, Luca Antiga, et al. Pytorch: An imperative style, high-performance deep learning library. *Advances in neural information processing systems (NeurIPS)*, 32, 2019. 4

[30] Joshua Robinson, Ching-Yao Chuang, Suvrit Sra, and Stefanie Jegelka. Contrastive learning with hard negative samples. In *International Conference on Learning Representation (ICLR)*, 2021. 1, 2, 4.2, 3, 4

[31] Olga Russakovsky, Jia Deng, Hao Su, Jonathan Krause, Sanjeev Satheesh, Sean Ma, Zhiheng Huang, Andrej Karpathy, Aditya Khosla, Michael Bernstein, et al. Imagenet large scale visual recognition challenge. *International journal of computer vision*, 115(3):211–252, 2015. 4.3

[32] Nikunj Saunshi, Orestis Plevrakis, Sanjeev Arora, Mikhail Khodak, and Hrishikesh Khande-parkar. A theoretical analysis of contrastive unsupervised representation learning. In *International Conference on Machine Learning (ICML)*, pages 5628–5637, 2019. 1

[33] Kihyuk Sohn. Improved deep metric learning with multi-class n-pair loss objective. *Advances in neural information processing systems (NeurIPS)*, 29:1857–1865, 2016. 1

[34] Yuval Tassa, Yotam Doron, Alistair Muldal, Tom Erez, Yazhe Li, Diego de Las Casas, David Budden, Abbas Abdolmaleki, Josh Merel, Andrew Lefrancq, et al. Deepmind control suite. *arXiv preprint arXiv:1801.00690*, 2018. 4.4

[35] Yonglong Tian, Dilip Krishnan, and Phillip Isola. Contrastive multiview coding. In *European Conference on Computer Vision (ECCV)*, pages 1–18, 2020. 1, 4.3, 3

[36] Yonglong Tian, Chen Sun, Ben Poole, Dilip Krishnan, Cordelia Schmid, and Phillip Isola. What makes for good views for contrastive learning. *Advances in Neural Information Processing Systems (NeurIPS)*, 33, 2020. 1

[37] Martin J Wainwright. *High-dimensional statistics: A non-asymptotic viewpoint*, volume 48. Cambridge University Press, 2019. 2.1

[38] Chen Wei, Huiyu Wang, Wei Shen, and Alan Yuille. Co2: Consistent contrast for unsupervised visual representation learning. In *International Conference on Learning Representations (ICLR)*, 2021. 4.3, 3

[39] Svante Wold, Kim Esbensen, and Paul Geladi. Principal component analysis. *Chemometrics and intelligent laboratory systems*, 2(1-3):37–52, 1987. 1.1

[40] Zhirong Wu, Yuanjun Xiong, Stella X Yu, and Dahua Lin. Unsupervised feature learning via non-parametric instance discrimination. In *IEEE Conference on Computer Vision and Pattern Recognition (CVPR)*, pages 3733–3742, 2018. 1, 1.1

[41] Lee Xiong, Chenyan Xiong, Ye Li, Kwok-Fung Tang, Jialin Liu, Paul Bennett, Junaid Ahmed, and Arnold Overwijk. Approximate nearest neighbor negative contrastive learning for dense text retrieval. *arXiv preprint arXiv:2007.00808*, 2020. 1

[42] Xinyi Xu, Cheng Deng, Yaochen Xie, and Shuiwang Ji. Group contrastive self-supervised learning on graphs. *IEEE Transactions on Pattern Analysis and Machine Intelligence*, 2022. 1

[43] Jiexi Yan, Cheng Deng, and Xianglong Liu. Dictionary learning in optimal metric space. In *Proceedings of the AAAI Conference on Artificial Intelligence (AAAI)*, volume 32, 2018. 1

[44] Jiexi Yan, Lei Luo, Cheng Deng, and Heng Huang. Unsupervised hyperbolic metric learning. In *Proceedings of the IEEE/CVF Conference on Computer Vision and Pattern Recognition (CVPR)*, pages 12465–12474, 2021. 1

[45] Jian Yang, David Zhang, Alejandro F Frangi, and Jing-yu Yang. Two-dimensional pca: a new approach to appearance-based face representation and recognition. *IEEE transactions on pattern analysis and machine intelligence*, 26(1):131–137, 2004. 1.1

[46] Huasong Zhong, Chong Chen, Zhongming Jin, and Xian-Sheng Hua. Deep robust clustering by contrastive learning. *arXiv preprint arXiv:2008.03030*, 2020. 1

[47] Jinguo Zhu, Shixiang Tang, Dapeng Chen, Shijie Yu, Yakun Liu, Mingzhe Rong, Aijun Yang, and Xiaohua Wang. Complementary relation contrastive distillation. In *IEEE Conference on Computer Vision and Pattern Recognition (CVPR)*, pages 9260–9269, 2021. 1, 4.3

[48] Martin Zinkevich, Markus Weimer, Alexander J Smola, and Lihong Li. Parallelized stochastic gradient descent. In *Advances in neural information processing systems (NeurIPS)*, volume 4, page 4, 2010. 2.3

Checklist

1. For all authors...
   (a) Do the main claims made in the abstract and introduction accurately reflect the paper's contributions and scope? [Yes]
   (b) Did you describe the limitations of your work? [Yes] See Section 5.
   (c) Did you discuss any potential negative societal impacts of your work? [N/A]
   (d) Have you read the ethics review guidelines and ensured that your paper conforms to them? [Yes]

2. If you are including theoretical results...
   (a) Did you state the full set of assumptions of all theoretical results? [Yes] See Theorem1/2/3.
   (b) Did you include complete proofs of all theoretical results? [Yes] See the Appendix in the supplementary material.

3. If you ran experiments...
   (a) Did you include the code, data, and instructions needed to reproduce the main experimental results (either in the supplemental material or as a URL)?[Yes] See Section 4 and supplemental material.
   (b) Did you specify all the training details (e.g., data splits, hyperparameters, how they were chosen)? [Yes] See Section 4.
   (c) Did you report error bars (e.g., with respect to the random seed after running experiments multiple times)? [Yes] See Section 4.
   (d) Did you include the total amount of compute and the type of resources used (e.g., type of GPUs, internal cluster, or cloud provider)? [Yes] See Section 4 and the supplyment material.

4. If you are using existing assets (e.g., code, data, models) or curating/releasing new assets...
   (a) If your work uses existing assets, did you cite the creators? [Yes]
   (b) Did you mention the license of the assets? [N/A]
   (c) Did you include any new assets either in the supplemental material or as a URL? [N/A]

   (d) Did you discuss whether and how consent was obtained from people whose data you're using/curating? [N/A]
   (e) Did you discuss whether the data you are using/curating contains personally identifiable information or offensive content? [N/A]

5. If you used crowdsourcing or conducted research with human subjects...
   (a) Did you include the full text of instructions given to participants and screenshots, if applicable? [N/A]
   (b) Did you describe any potential participant risks, with links to Institutional Review Board (IRB) approvals, if applicable? [N/A]
   (c) Did you include the estimated hourly wage paid to participants and the total amount spent on participant compensation? [N/A]

Appendix for
"Learning Contrastive Embedding
in Low-Dimensional Space"

Shuo Chen[†]**, Chen Gong**[§]**, Jun Li**[§]**, Jian Yang**[§]**, Gang Niu**[†]**, Masashi Sugiyama**[‡]

Abstract

This supplementary document contains additional experiments and all technical proofs for **Theorem 2** and **Theorem 3** in the *NeurIPS'22* paper entitled "Learning Contrastive Embedding in Low-Dimensional Space". It is indeed the appendix section of the paper. Source code is available at https://github.com/functioncs/CLLR.

A. Additional Experiments

A.1. Parametric Sensitivity

Here we investigate the parametric sensitivities of λ and α in our method. Specifically, we change λ and α in $[0.01, 5]$ and $[1, 20]$, respectively, and we record the classification accuracy of our method on *STL-10* dataset (batch size=256, epochs=100). Tab. 0.1 clearly shows that the accuracy variation of our method is smaller than 1.5.

Similar experiments are conducted on *CIFAR-10* dataset, where we can observe that the accuracy variation of our method is smaller than 2.0. These results clearly demonstrate that the two regularization parameters λ and α are very stable within a given range. It implies that the hyper-parameters of our method can be easily tuned in practice use.

Table 0.1: Parametric sensitivities of λ and α on *STL-10* dataset. Here λ and α are changed in $[0.01, 5]$ and $[1, 20]$, respectively.

λ \ α	1	5	10	15	20
0.01	78.4	79.3	79.2	78.2	78.0
0.1	78.2	79.1	79.2	78.8	77.9
0.5	77.8	78.6	79.2	<u>**79.4**</u>	79.2
5	78.9	78.9	78.9	78.6	<u>**79.4**</u>

Table 0.2: Parametric sensitivities of λ and α on *CIFAR-10* dataset. Here λ and α are changed in $[0.01, 5]$ and $[1, 20]$, respectively.

λ \ α	1	5	10	15	20
0.01	93.8	94.3	94.2	<u>**95.2**</u>	94.1
0.1	94.2	95.1	<u>**95.2**</u>	<u>**95.2**</u>	94.2
0.5	93.8	93.6	93.2	93.4	94.2
5	93.9	94.9	94.9	94.6	94.4

Table 0.3: Training time of the baseline methods and our proposed method (100 epochs, in hours).

Method	*CIFAR-10*		*ImageNet-100*	
	512	1024	512	1024
SimCLR [3]	2.3	1.3	10.9	5.5
DCL [5]	2.5	1.4	11.2	5.7
CLLR(SimCLR+$\ell_{2,1}$-norm)	2.3	1.4	10.9	5.6
CLLR(SimCLR+nuclear-norm)	2.4	1.5	11.2	5.8
CLLR(DCL+$\ell_{2,1}$-norm)	2.5	1.6	11.3	5.8
CLLR(DCL+nuclear-norm)	2.6	1.6	11.5	5.9

A.2. Running Time Comparsion

As we described in the manuscript, we adopt the sub-gradients of $\ell_{2,1}$-norm and nuclear-norm as the stochastic gradients during the iteration. However, the iteration of nuclear-norm may be time-consuming which involves the s*ingular value decomposition* (SVD) operation [1]. Therefore, here we further provide experiments to record the training time of our method as well as the corresponding baseline method. Specifically,we use four NVIDIA TeslaV100 GPUs to train our method based on SimCLR and DCL with 100 epochs, where the batch size is set to 512 and 1024.

In Tab. 0.3, we can find that the proposed regularizer only brings in little additional time consumption. This is because the gradient calculations of $\ell_{2,1}$-norm $\|\boldsymbol{L}\|_{2,1}$ and nuclear-norm $\|\boldsymbol{L}\|_*$ are independent to the size of training data, so the training time is still acceptable in practice use.

A.3. Comparison with Distillation-Based Contrastive Learning

We may notice that the distillation method can also reduce the dimensionality of contrastive embeddings. However, in the distillation-based CL, the distilled student model is usually supervised by the original teacher model, so the distillation-based CL may naturally inherit improper similarities learned by the original CL. In comparison, our CLLR directly reduces the feature dimensionality of the original CL to avoid / alleviate the improper similarity measure. Therefore, it is worth pointing out that our method is completely different from the distillation-based CL methods.

Here we further provide experiments in Tab. 0.4 to compare our method with the distillation-based CL methods. We select the recent works *wasserstein contrastive representation distillation* (WCoRD) [2] and *complementary relation contrastive distillation* (CRCD) [8]for comparsions, where the output dimensionlaities of their student networks are set to 256-dimension and 512-dimension. We can find that most distilled student models have the close or slightly lower classification accuracy compared with the corresponding baseline teacher models (as reported in their original paper). In comparison, our method can consistently improve the baseline method on all three datasets. Meanwhile, we observe that our method significantly outperforms the distillation-based methods in both 256-dimension and 512-dimension settings.

A.4. Experiments on Negative-Free Contrastive Learning

Although we implement our method on CL models that use both positive and negative samples, our proposed CLLR can also work with negative-free models. We follow the reviewer's suggestion

Table 0.4: Classification accuracy (%, Top5) of the distillation-based methods and our proposed method on *STL-10*, *CIFAR-10*, and *ImageNet-100* datasets (batch size = 512 / 1024, epochs = 500).

Method	STL-10		CIFAR-10		ImageNet-100	
	512	1024	512	1024	512	1024
SimCLR (Teacher)	81.3	82.3	91.3	93.3	77.9	80.5
WCoRD(256-dimension) [2]	80.2	81.3	90.3	90.3	76.9	75.5
WCoRD(512-dimension) [2]	81.2	81.4	92.5	91.4	77.2	79.7
CRCD(256-dimension) [8]	79.4	80.3	89.3	91.3	74.9	81.5
CRCD(512-dimension) [8]	81.4	82.4	92.0	90.4	78.2	79.7
CLLR(SimCLR+nuclear-norm, 256-dimension)	**85.2**	86.4	**93.7**	96.4	**81.2**	84.6
CLLR(SimCLR+nuclear-norm, 512-dimension)	84.4	**87.1**	93.3	**96.5**	80.9	**84.8**

Table 0.5: Classification accuracy (%, Top1 and Top5) of combining our proposed method with negative-free contrastive learning methods on *ImageNet-100* dataset (batch size = 1024 / 4096, epochs = 500).

Method	1024		4096	
	Top1	Top5	Top1	Top5
BYOL [6]	61.3	91.8	74.9	91.9
SimSiam [4]	70.9	91.9	73.6	92.8
CLLR(BYOL+nuclear-norm)	63.1	92.7	**76.5**	93.0
CLLR(SimSiam+nuclear-norm)	**72.2**	**92.9**	75.8	**93.8**

to conduct experiments on negative-free CL baselines (BYOL [6] and SimSiam [4], merely using positive pairs) to validate the effectiveness of our proposed method. As shown in Tab. 0.5, our method can consistently improve the compared methods upon themselves (Top1 and Top5 accuracy on *ImageNet-100* with 500 training epochs and batch size = 1024 / 4096).

A.5. Training Models via Other Optimizers

Since our proposed reconstruction loss and regularizer are differentiable almost everywhere, we can employ some other optimizers such as Adam to minimize the learning objective of our CLLR. Specifically, here use the Adam optimizer to training our model on *CIFAR-10* dataset (batch size = 256), and we record the corresponding training / test errors (%) after 100, 200, and 400 epochs. In Tab. 0.6, we observe that both SGD (learning rate = 5×10^{-3}) and Adam can converge well after 400 epochs. Therefore, our proposed method has good compatibility with existing (stochastic) optimizers.

Table 0.6: Training / test errors (%, Top5) of our method by using SGD and Adam on *CIFAR-10* dataset.

Optimizer	100 epochs	200 epochs	300 epochs	400 epochs
SGD	30.2±5.3 / 35.8±4.3	10.8±2.1 / 15.8±2.3	3.3±1.8 / 10.4±2.3	2.1±1.1 / 6.9±1.3
Adam [7]	20.2±4.3 / 25.4±3.3	14.1±1.9 / 18.8±4.1	3.4±1.5 / 10.5±3.4	2.4±1.2 / 7.2±2.1

B. Proofs

B.1. Derivation for Eq. (3)

According to the definition of gamma function, we have that

$$\lim_{H \to \infty} (\pi^{H/2}/(H \cdot \Gamma(H/2)))/2^{H-1}$$

$$= \lim_{H \to \infty} (\pi^{H/2}/(H \cdot \int_0^\infty t^{H/2-1}\mathrm{e}^{-t}dt))/2^{H-1}$$

$$\leq \lim_{H \to \infty} (\pi^{H/2}/(H \cdot \int_1^2 t^{H/2-1}\mathrm{e}^{-t}dt))/2^{H-1}. \tag{0.1}$$

By further using the *mean-value theorem*, we have

$$\lim_{H \to \infty} (\pi^{H/2}/(H \cdot \int_1^2 t^{H/2-1}\mathrm{e}^{-t}dt))/2^{H-1}$$

$$\leq \lim_{H \to \infty} (\pi^{H/2}/(H \cdot \mathrm{e}^{-2}))/2^{H-1}$$

$$\leq \lim_{H \to \infty} \pi^{(H-1)/2}/2^{H-1}. \tag{0.2}$$

Finally, it is easy to obtain that

$$\lim_{H \to \infty} \pi^{(H-1)/2}/2^{H-1} = \lim_{H \to \infty} (\pi/4)^{(H-1)/2} = 0, \tag{0.3}$$

which is Eq. (3) in our manuscript.

B.2. Proof for Theorem 2

Theorem 2. *If the function $\mathcal{F}(\boldsymbol{\Phi}, \boldsymbol{L})$ has δ-bounded gradient (i.e., $\|\nabla\mathcal{F}(\boldsymbol{\Phi}, \boldsymbol{L})\|_2 < \delta$), then we let $\eta = \sqrt{2(\mathcal{F}(\boldsymbol{\Phi}_{(0)}, \boldsymbol{L}_{(0)}) - \mathcal{F}(\boldsymbol{\Phi}^*, \boldsymbol{L}^*))/(S\delta^2 T)}$, and for the iterations in Algorithm 1 we have that*

$$\min_{0 \leq t \leq T-1} \mathbb{E}[\|\nabla\mathcal{F}(\boldsymbol{\Phi}_{(t)}, \boldsymbol{L}_{(t)})\|_2]$$

$$\leq \sqrt{2S(\mathcal{F}(\boldsymbol{\Phi}_{(0)}, \boldsymbol{L}_{(0)}) - \mathcal{F}(\boldsymbol{\Phi}^*, \boldsymbol{L}^*))/T}\,\delta, \tag{0.4}$$

where $S > 0$ is the lipschitz constant such that $\|\nabla\mathcal{F}(\boldsymbol{\Phi}, \boldsymbol{L}) - \nabla\mathcal{F}(\boldsymbol{\Phi}', \boldsymbol{L}')\|_2 \leq S\|[\boldsymbol{\Phi}, \boldsymbol{L}] - [\boldsymbol{\Phi}', \boldsymbol{L}']\|_2$.

Proof. Firstly, by using the lipschitz continuity of $\mathcal{F}(\boldsymbol{\Phi}, \boldsymbol{L})$ we have that

$$\mathbb{E}[\mathcal{F}(\boldsymbol{\Phi}_{(t+1)}, \boldsymbol{L}_{(t+1)})] - \mathbb{E}[\mathcal{F}(\boldsymbol{\Phi}_{(t)}, \boldsymbol{L}_{(t)})]$$

$$\leq \mathbb{E}[\|\nabla\mathcal{F}(\boldsymbol{\Phi}_{(t+1)}, \boldsymbol{L}_{(t+1)}) - ([\boldsymbol{\Phi}_{(t+1)}, \boldsymbol{L}_{(t+1)}] - [\boldsymbol{\Phi}_{(t)}, \boldsymbol{L}_{(t)}])\|_2^2$$

$$+ S/2\|[\boldsymbol{\Phi}_{(t+1)}, \boldsymbol{L}_{(t+1)}] - [\boldsymbol{\Phi}_{(t)}, \boldsymbol{L}_{(t)}]\|_2^2]$$

$$\leq -\eta_t\mathbb{E}[\nabla\mathcal{F}(\boldsymbol{\Phi}_{(t)}, \boldsymbol{L}_{(t)})\|_2^2] + (S\eta_t^2/2)\mathbb{E}[\|\nabla\mathcal{F}_{b_i}(\boldsymbol{\Phi}_{(t)}, \boldsymbol{L}_{(t)})\|_2^2]$$

$$\leq -\eta_t\mathbb{E}[\nabla\mathcal{F}(\boldsymbol{\Phi}_{(t)}, \boldsymbol{L}_{(t)})\|_2^2] + (S\eta_t^2/2)\delta^2, \tag{0.5}$$

where the second inequality follows from the fact that $[\boldsymbol{\Phi}_{(t+1)}, \boldsymbol{L}_{(t+1)}]$ is updated by Algorithm 1. Then, we have that

$$\mathbb{E}[\nabla\mathcal{F}(\boldsymbol{\Phi}_{(t)}, \boldsymbol{L}_{(t)})\|_2^2] \leq (1/\eta_t)\mathbb{E}[\mathcal{F}(\boldsymbol{\Phi}_{(t)}, \boldsymbol{L}_{(t)}) - \mathcal{F}(\boldsymbol{\Phi}_{(t+1)}, \boldsymbol{L}_{(t+1)})] + (L\eta_t/2)\delta^2, \tag{0.6}$$

and thus

$$\begin{cases} \mathbb{E}[\nabla\mathcal{F}(\boldsymbol{\Phi}_{(0)}, \boldsymbol{L}_{(0)})\|_2^2] \leq (1/\eta_0)\mathbb{E}[\mathcal{F}(\boldsymbol{\Phi}_{(0)}, \boldsymbol{L}_{(0)}) - \mathcal{F}(\boldsymbol{\Phi}_{(1)}, \boldsymbol{L}_{(1)})] + (S\eta_0/2)\delta^2, \\ \mathbb{E}[\nabla\mathcal{F}(\boldsymbol{\Phi}_{(1)}, \boldsymbol{L}_{(1)})\|_2^2] \leq (1/\eta_1)\mathbb{E}[\mathcal{F}(\boldsymbol{\Phi}_{(1)}, \boldsymbol{L}_{(1)}) - \mathcal{F}(\boldsymbol{\Phi}_{(2)}, \boldsymbol{L}_{(2)})] + (S\eta_1/2)\delta^2, \\ ... \\ \mathbb{E}[\nabla\mathcal{F}(\boldsymbol{\Phi}_{(T-1)}, \boldsymbol{L}_{(T-1)})\|_2^2] \leq \frac{1}{\eta_{T-1}}\mathbb{E}[\mathcal{F}(\boldsymbol{\Phi}_{(T-1)}, \boldsymbol{L}_{(T-1)}) - \mathcal{F}(\boldsymbol{\Phi}_{(T)}, \boldsymbol{L}_{(T)})] + \frac{S\eta_{T-1}}{2}\delta^2. \end{cases} \tag{0.7}$$

Finally, we sum all inequalities in the above Eq. (0.7) and letting $\eta_0 = \eta_1 = \cdots = \eta_{T-1} = \eta$. Then we have

$$
\min_{0 \leq t \leq T-1} \mathbb{E}[\,\|\nabla \mathcal{F}(\boldsymbol{\Phi}_{(t)}, \boldsymbol{L}_{(t)})\|_2]
$$

$$
\leq \frac{1}{T} \sum_{t=0}^{T-1} \mathbb{E}[\,\|\nabla \mathcal{F}(\boldsymbol{\Phi}_{(t)}, \boldsymbol{L}_{(t)})\|_2] + (S\eta/2)\delta^2
$$

$$
\leq \frac{1}{T\eta} \mathbb{E}[\mathcal{F}(\boldsymbol{\Phi}_{(0)}, \boldsymbol{L}_{(t)}) - \mathcal{F}(\boldsymbol{\Phi}_{(t)}, \boldsymbol{L}_{(t)})] + (S\eta/2)\delta^2
$$

$$
\leq \frac{1}{T\eta} (\mathcal{F}(\boldsymbol{\Phi}_{(0)}, \boldsymbol{L}_{(t)}) - \mathcal{F}(\boldsymbol{\Phi}^*, \boldsymbol{L}^*)) + (S\eta/2)\delta^2
$$

$$
\leq \frac{1}{\sqrt{T}} ((\mathcal{F}(\boldsymbol{\Phi}_{(0)}, \boldsymbol{L}_{(t)}) - \mathcal{F}(\boldsymbol{\Phi}^*, \boldsymbol{L}^*))/c + (Sc/2)\delta^2), \qquad (0.8)
$$

where $c = \eta\sqrt{T}$. We set $c = \sqrt{2(\mathcal{F}(\boldsymbol{\Phi}_{(0)}, \boldsymbol{L}_{(0)}) - \mathcal{F}(\boldsymbol{\Phi}^*, \boldsymbol{L}^*))/(S\delta^2)}$, and we have

$$
\min_{0 \leq t \leq T-1} \mathbb{E}[\,\|\nabla \mathcal{F}(\boldsymbol{\Phi}_{(t)}, \boldsymbol{L}_{(t)})\|_2] \leq \sqrt{2S(\mathcal{F}(\boldsymbol{\Phi}_{(0)}, \boldsymbol{L}_{(0)}) - \mathcal{F}(\boldsymbol{\Phi}^*, \boldsymbol{L}^*))/T}\,\delta, \qquad (0.9)
$$

which completes the proof. $\qquad\square$

B.3. Proof for Theorem 3

Theorem 3. *For any given $n + 1$ i.i.d. random data points $\boldsymbol{x}, \boldsymbol{x}_1, \boldsymbol{x}_2, \ldots, \boldsymbol{x}_n \in \mathbb{R}^m$, we denote that $\mathcal{D}_{\widehat{\boldsymbol{\Phi}}, \widehat{\boldsymbol{L}}}^{\max} = \max\{\mathcal{D}_{\widehat{\boldsymbol{\Phi}}, \widehat{\boldsymbol{L}}}(\boldsymbol{x}, \boldsymbol{x}_i) | i = 1, 2, \ldots, n\}$ and $\mathcal{D}_{\widehat{\boldsymbol{\Phi}}, \widehat{\boldsymbol{L}}}^{\min} = \min\{\mathcal{D}_{\widehat{\boldsymbol{\Phi}}, \widehat{\boldsymbol{L}}}(\boldsymbol{x}, \boldsymbol{x}_i) | i = 1, 2, \ldots, n\}$, and we have that*

$$
\mathcal{P}\left\{ (\mathcal{D}_{\widehat{\boldsymbol{\Phi}}, \widehat{\boldsymbol{L}}}^{\max} - \mathcal{D}_{\widehat{\boldsymbol{\Phi}}, \widehat{\boldsymbol{L}}}^{\min})/\mathcal{D}_{\widehat{\boldsymbol{\Phi}}, \widehat{\boldsymbol{L}}}^{\min} \geq \alpha\lambda C(\mathcal{X}) \right\} = 1, \qquad (0.10)
$$

where $\mathcal{D}_{\widehat{\boldsymbol{\Phi}}, \widehat{\boldsymbol{L}}}(\boldsymbol{x}, \boldsymbol{x}_i) = \|\widehat{\boldsymbol{L}}\widehat{\boldsymbol{\Phi}}(\boldsymbol{x}) - \widehat{\boldsymbol{L}}\widehat{\boldsymbol{\Phi}}(\boldsymbol{x}_i)\|_2/\mathrm{rank}(\widehat{\boldsymbol{L}})$, and parameters $\widehat{\boldsymbol{\Phi}}$ and $\widehat{\boldsymbol{L}}$ are learned from Eq. (13).

Proof. As $\widehat{\boldsymbol{\Phi}}$ and $\widehat{\boldsymbol{L}}$ are iterated by the optimization algorithm, we have

$$
\mathcal{L}_{\mathrm{NCE}}(\widehat{\boldsymbol{\Phi}}) + \lambda\mathbb{E}_{\boldsymbol{x} \in \mathcal{X}}[\,\|\widehat{\boldsymbol{L}}^\top \widehat{\boldsymbol{L}} \cdot \widehat{\boldsymbol{\Phi}}(\boldsymbol{x}) - \widehat{\boldsymbol{\Phi}}(\boldsymbol{x})\|_2^2] + \alpha\lambda\mathcal{R}(\widehat{\boldsymbol{\Phi}}, \widehat{\boldsymbol{L}})
$$

$$
\leq \mathcal{L}_{\mathrm{NCE}}(\boldsymbol{\Phi}_{(0)}) + \lambda\mathbb{E}_{\boldsymbol{x} \in \mathcal{X}}[\,\|\boldsymbol{L}_{(0)}^\top \boldsymbol{L}_{(0)} \cdot \boldsymbol{\Phi}_{(0)}(\boldsymbol{x}) - \boldsymbol{\Phi}_{(0)}(\boldsymbol{x})\|_2^2] + \alpha\lambda\mathcal{R}(\boldsymbol{\Phi}_{(0)}, \boldsymbol{L}_{(0)}), \qquad (0.11)
$$

which implies that

$$
\mathcal{R}(\widehat{\boldsymbol{\Phi}}, \widehat{\boldsymbol{L}}) \leq \frac{1}{\alpha\lambda}\left(\mathcal{F}(\boldsymbol{\Phi}_{(0)}, \boldsymbol{L}_{(0)}) - \mathcal{L}_{\mathrm{NCE}}(\widehat{\boldsymbol{\Phi}}) - \lambda\mathbb{E}_{\boldsymbol{x} \in \mathcal{X}}[\,\|\widehat{\boldsymbol{L}}^\top \widehat{\boldsymbol{L}} \cdot \widehat{\boldsymbol{\Phi}}(\boldsymbol{x}) - \widehat{\boldsymbol{\Phi}}(\boldsymbol{x})\|_2^2] \right)
$$

$$
= \frac{1}{\alpha\lambda}c_1 - \frac{1}{\alpha}c_2 + c_3
$$

$$
= \frac{1}{\alpha}\left(\frac{1}{\lambda}c_1 - c_2 \right) + c_3, \qquad (0.12)
$$

where

$$
\begin{cases}
c_1 = \mathcal{L}_{\mathrm{NCE}}(\boldsymbol{\Phi}_{(0)}) - \mathcal{L}_{\mathrm{NCE}}(\widehat{\boldsymbol{\Phi}}), \\
c_2 = \mathbb{E}_{\boldsymbol{x} \in \mathcal{X}}[\,\|\boldsymbol{L}_{(0)}^\top \boldsymbol{L}_{(0)} \cdot \boldsymbol{\Phi}_{(0)}(\boldsymbol{x}) - \boldsymbol{\Phi}_{(0)}(\boldsymbol{x})\|_2^2] - \mathbb{E}_{\boldsymbol{x} \in \mathcal{X}}[\,\|\widehat{\boldsymbol{L}}^\top \widehat{\boldsymbol{L}} \cdot \widehat{\boldsymbol{\Phi}}(\boldsymbol{x}) - \widehat{\boldsymbol{\Phi}}(\boldsymbol{x})\|_2^2], \\
c_3 = \mathcal{R}(\boldsymbol{\Phi}_{(0)}, \boldsymbol{L}_{(0)}).
\end{cases} \qquad (0.13)
$$

Then we have that $\|\widehat{\boldsymbol{L}}\|_{2,1} \leq \frac{1}{\alpha}\left(\frac{1}{\lambda}c_1 - c_2 \right) + c_3$ and $\|\widehat{\boldsymbol{L}}\|_* \leq \frac{1}{\alpha}\left(\frac{1}{\lambda}c_1 - c_2 \right) + c_3$, respectively. Therefore, we have $\|\widehat{\boldsymbol{L}}\|_{2,0} \leq k_1\left(\frac{1}{\alpha}\left(\frac{1}{\lambda}c_1 - c_2 \right) + c_3 \right)$ and $\mathrm{rank}(\widehat{\boldsymbol{L}}) \leq k_2\left(\frac{1}{\alpha}\left(\frac{1}{\lambda}c_1 - c_2 \right) + c_3 \right)$. It

implies that the pairwise distance $\mathcal{D}_{\widehat{\boldsymbol{\Phi}},\widehat{\boldsymbol{L}}}(\boldsymbol{x},\,\boldsymbol{x}_i)$ satisfies that

$$\frac{\mathcal{D}_{\widehat{\boldsymbol{\Phi}},\widehat{\boldsymbol{L}}}^{\max} - \mathcal{D}_{\widehat{\boldsymbol{\Phi}},\widehat{\boldsymbol{L}}}^{\min}}{\mathcal{D}_{\widehat{\boldsymbol{\Phi}},\widehat{\boldsymbol{L}}}^{\min}}$$

$$= \frac{\max_{i=1,\ldots,n}\sqrt{\sum_{j=1}^{H}(\widehat{\boldsymbol{L}}^{(j)}\widehat{\boldsymbol{\Phi}}(\boldsymbol{x}) - \widehat{\boldsymbol{L}}^{(j)}\widehat{\boldsymbol{\Phi}}(\boldsymbol{x}_i))}/\mathrm{rank}(\widehat{\boldsymbol{L}}) - \min_{i=1,\ldots,n}\sqrt{\sum_{j=1}^{H}(\widehat{\boldsymbol{L}}^{(j)}\widehat{\boldsymbol{\Phi}}(\boldsymbol{x}) - \widehat{\boldsymbol{L}}^{(j)}\widehat{\boldsymbol{\Phi}}(\boldsymbol{x}_i))}/\mathrm{rank}(\widehat{\boldsymbol{L}})}{\min_{i=1,2,\ldots,n}\sqrt{\sum_{j=1}^{H}(\widehat{\boldsymbol{L}}^{(j)}\widehat{\boldsymbol{\Phi}}(\boldsymbol{x}) - \widehat{\boldsymbol{L}}^{(j)}\widehat{\boldsymbol{\Phi}}(\boldsymbol{x}_i))}/\mathrm{rank}(\widehat{\boldsymbol{L}})}$$

$$= \frac{\max_{i=1,2,\ldots,n}\sqrt{\sum_{j=1}^{H}(\widehat{\boldsymbol{L}}^{(j)}\widehat{\boldsymbol{\Phi}}(\boldsymbol{x}) - \widehat{\boldsymbol{L}}^{(j)}\widehat{\boldsymbol{\Phi}}(\boldsymbol{x}_i))}/\mathrm{rank}(\widehat{\boldsymbol{L}})}{\min_{i=1,2,\ldots,n}\sqrt{\sum_{j=1}^{H}(\widehat{\boldsymbol{L}}^{(j)}\widehat{\boldsymbol{\Phi}}(\boldsymbol{x}) - \widehat{\boldsymbol{L}}^{(j)}\widehat{\boldsymbol{\Phi}}(\boldsymbol{x}_i))}/\mathrm{rank}(\widehat{\boldsymbol{L}})} - 1$$

$$\geq \frac{\max_{i=1,2,\ldots,n}\sqrt{\sum_{j=1}^{H}(\widehat{\boldsymbol{L}}^{(j)}\widehat{\boldsymbol{\Phi}}(\boldsymbol{x}) - \widehat{\boldsymbol{L}}^{(j)}\widehat{\boldsymbol{\Phi}}(\boldsymbol{x}_i))}/k_2\left(\frac{1}{\alpha}\left(\frac{1}{\lambda}c_1 - c_2\right) + c_3\right)}{\min_{i=1,2,\ldots,n}\sqrt{\sum_{j=1}^{H}(\widehat{\boldsymbol{L}}^{(j)}\widehat{\boldsymbol{\Phi}}(\boldsymbol{x}) - \widehat{\boldsymbol{L}}^{(j)}\widehat{\boldsymbol{\Phi}}(\boldsymbol{x}_i))}/\mathrm{rank}(\widehat{\boldsymbol{L}})}$$

$$= \frac{Q}{k_2\left(\frac{1}{\alpha}\left(\frac{1}{\lambda}c_1 - c_2\right) + c_3\right)}$$

$$\geq \frac{\alpha\lambda Q}{k_2 c_1}, \tag{0.14}$$

where

$$Q = \frac{\max_{i=1,2,\ldots,n}\sqrt{\sum_{j=1}^{H}(\widehat{\boldsymbol{L}}^{(j)}\widehat{\boldsymbol{\Phi}}(\boldsymbol{x}) - \widehat{\boldsymbol{L}}^{(j)}\widehat{\boldsymbol{\Phi}}(\boldsymbol{x}_i))}}{\min_{i=1,2,\ldots,n}\sqrt{\sum_{j=1}^{H}(\widehat{\boldsymbol{L}}^{(j)}\widehat{\boldsymbol{\Phi}}(\boldsymbol{x}) - \widehat{\boldsymbol{L}}^{(j)}\widehat{\boldsymbol{\Phi}}(\boldsymbol{x}_i))}/\mathrm{rank}(\widehat{\boldsymbol{L}})}. \tag{0.15}$$

Finally, we let $C(\mathcal{X}) = Q/(k_2 c_1)$ and complete the proof. $\square$

References

[1] Stephen Boyd, Stephen P Boyd, and Lieven Vandenberghe. *Convex optimization*. Cambridge university press, 2004. (document)

[2] Liqun Chen, Dong Wang, Zhe Gan, Jingjing Liu, Ricardo Henao, and Lawrence Carin. Wasserstein contrastive representation distillation. In *IEEE Conference on Computer Vision and Pattern Recognition (CVPR)*, pages 16296–16305, 2021. (document), 0.4

[3] Ting Chen, Simon Kornblith, Mohammad Norouzi, and Geoffrey Hinton. A simple framework for contrastive learning of visual representations. In *International Conference on Machine Learning (ICML)*, pages 1597–1607, 2020. 0.3

[4] Xinlei Chen and Kaiming He. Exploring simple siamese representation learning. In *IEEE Conference on Computer Vision and Pattern Recognition (CVPR)*, pages 15750–15758, 2021. 0.5, (document)

[5] Ching-Yao Chuang, Joshua Robinson, Lin Yen-Chen, Antonio Torralba, and Stefanie Jegelka. Debiased contrastive learning. *Advances in Neural Information Processing Systems (NeurIPS)*, 33, 2020. 0.3

[6] Jean-Bastien Grill, Florian Strub, Florent Altche, Corentin Tallec, Pierre Richemond, Elena Buchatskaya, Carl Doersch, Bernardo Avila Pires, Zhaohan Guo, Mohammad Gheshlaghi Azar, et al. Bootstrap your own latent-a new approach to self-supervised learning. *Advances in Neural Information Processing Systems (NeurIPS)*, 33:21271–21284, 2020. 0.5, (document)

[7] Sashank J Reddi, Satyen Kale, and Sanjiv Kumar. On the convergence of adam and beyond. In *International Conference on Learning Representations (ICLR)*, 2018. 0.6

[8] Jinguo Zhu, Shixiang Tang, Dapeng Chen, Shijie Yu, Yakun Liu, Mingzhe Rong, Aijun Yang, and Xiaohua Wang. Complementary relation contrastive distillation. In *IEEE Conference on Computer Vision and Pattern Recognition (CVPR)*, pages 9260–9269, 2021. (document), 0.4